Analysis, Modeling and Implementation of a Switching Bi-Directional Buck-Boost Converter Based on Electric Vehicle Hybrid Energy Storage for V2G System

SHUO LIU[ID]1**, XU XIE**[ID]1**, AND LIYONG YANG**[ID]2

[1]Electrical and Control Engineering College, North China University of Technology, Beijing 100144, China
[2]Beijing Electric Power Energy-Saving Key Technology Collaborative Innovation Center, North China University of Technology, Beijing 100144, China

Corresponding author: Xu Xie (2018311010112@mail.ncut.edu.cn)

ABSTRACT This paper presents a switching bi-directional buck-boost converter (SBBBC) for vehicles-to-grid (V2G) system. The topology can provide an energy bi-directional flow path for energy exchange between the Li-battery/supercapacitor (SC) hybrid energy storage system (HESS) of the electric vehicle and the grid. This topology not only has buck-boost capability, but also has the function of energy management. In this paper, the state-space averaging method is used to analyze the stability of the topology in boost and buck modes. The control strategy is given according to the state of charge (SOC) of the energy storage system to ensure that the output voltage and current are stable. And the Li-battery is charged in constant current (CC) and constant voltage (CV) mode. The voltage and current controllers are designed in the frequency domain based on bode plots. Finally, the electrical feasibility of the topology, the suitability of the design controller and control strategy are verified by simulation and experiment.

INDEX TERMS Switching bi-directional buck-boost converter, hybrid energy storage system, Li-battery, supercapacitors, V2G.

I. INTRODUCTION

Electric vehicles have been widely used because of their cleanliness and low impact on the environment [1]. Li-batteries are of critical importance part in energy storage systems of electric vehicle [2]. Although Li-batteries with high energy densities can provide enough energy during steady-state operation, the power densities of Li-batteries are too low to meet the peak power demand [3], [4]. Combining Li-batteries and supercapacitors (SC) to form a hybrid energy storage system (HESS) can solve the problem. The reason is that SC with higher power densities can provide the transient power required by the load [5]–[17].

Since output voltage peak of the voltage source inverter is less than the dc-link side voltage, it is necessary to use the dc-dc converter to raise the Li-battery voltage [18]. Figure 1 shows the block diagram of HESS. The SC is

The associate editor coordinating the review of this manuscript and approving it for publication was Yunfeng Wen[ID].
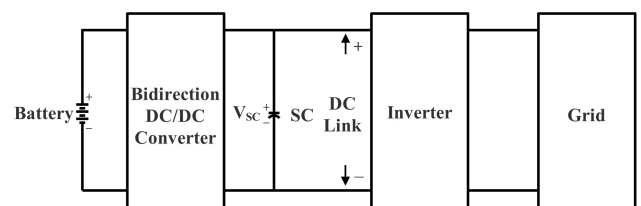

FIGURE 1. The block diagram of HESS.

directly connected to the inverter, which can increase the dynamic response of the HESS during transient peak power demand, while the Li-battery is connected to the DC-link by a bi-directional DC/DC converter [19]. The effect of the bi-directional dc-dc converter in the HESS is to transfer the energy and keep the dc bus voltage stability. Moreover, the converter should provide bi-directional power flow because the energy storage system and the grid require energy exchange [20].

A HESS topology is mentioned in articles [3] and [5]. In the topology of [3] and [5], the Li-battery can be connected to the SC via a bi-directional dc-dc half-bridge or directly to the DC bus via a diode. This two-stage converter can make full use of the power capacity of the SC but the boost ratio is low. A buck-boost converter for a plug-in hybrid electric vehicle is proposed in paper [21] and [22], respectively. However, the converter mentioned in the paper [21] cannot achieve a bi-directional flow of energy between the grid and the energy storage device. The converter mentioned in the paper [22] has many switching devices, large losses and complicated control. A high voltage gain bi-directional dc-dc converter is given in article [23]. This topology can operate under zero voltage switching conditions and reduces switching and conduction losses. However, this topology has many switching states and the operation is complicated.

In [13] and [24], hybrid energy storage systems for electric vehicles based on Z-source inverters (ZSI) and quasi-Z-source inverters (qZSI) were proposed. These two topologies have the boost capability, and provide a bi-directional energy flow path. Moreover, the reliability of the hybrid energy storage system is enhanced due to the characteristics that allow the inverter to shoot-through. These two topologies can increase power density [25]. The control strategies proposed in [13] and [24] are complex, and the topologies have multiple passive components between the SC and the DC bus, which will greatly increase the size of the device.

This paper proposes a switching bi-directional buck-boost converter (SBBBC) and its appropriate control strategy, which is used in the HESS for vehicles-to-grid (V2G) system. The converter allows shoot-through of two switches of any phase, with anti-electromagnetic interference capability. Meanwhile, since there are three switches in the DC side, the SC and Li-battery can fulfill bi-directional power flow. Furthermore, the small-signal model of the topology is established by state space averaging method and the stability of the system is analyzed. The control strategy is given according to the state of charge (SOC) of the energy storage system and the operating state of the circuit. The performance of the proposed converter and control strategy are verified through simulation and experimental results.

II. TOPOLOGY AND MODULATION OF THE PROPOSED SWITCHING BI-DIRECTION BUCK-BOOST CONVERTER
A. PROPOSED TOPOLOGY
Figure 2 shows the proposed SBBBC with HESS, which consists of five parts: Li-battery, switching bi-directional buck-boost circuit, SC, full bridge inverter and gird. The switching bi-directional buck-boost circuit has an inductor, a SC and the additional three switches (S_{D1}, S_{D2}, S_{D3}). Since the gate signals of switches S_{D2} and S_{D3} are the same and complementary to the gate signal of switch S_{D1}, one gate signal can control these three additional switches. This unique SBBBC network allows the system work on the buck and boost modes, and it can provide bi-directional power flow.
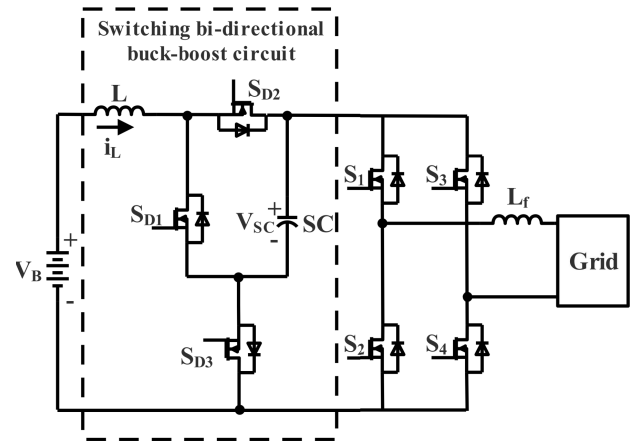

FIGURE 2. The proposed SBBBC.

TABLE 1. Switch combination and inverter output voltage.

N	U_{AC}	S_{D1},S_{D2},S_{D3}	S_1,S_3	S_2,S_4	state
1	0	0 1 1	0 0	1 1	zero state
2	0	0 1 1	1 1	0 0	zero state
3	$-U_{SC}$	0 1 1	0 1	1 0	active state
4	U_{SC}	0 1 1	1 0	0 1	active state
5	0	1 0 0	1 1	X X	shoot-through state
6	0	1 0 0	X X	1 1	shoot-through state

Note: X is 0 or 1.

B. MODULATION METHOD
In the proposed converter, there are three switching-states include active state, zero state and shoot-through state respectively, as shown in Table 1. All switches of full bridge inverter are operated in the SPWM mode to modulate output voltage. The switching bi-directional buck-boost circuit uses the shoot-through duty to achieve buck-boost voltage.

The duty cycle is calculated by:

$$\begin{cases} d = m\sin(\theta) \\ d_s = const \qquad (d_s \le 1 - d) \\ d_0 = 1 - d - d_s \end{cases} \qquad (1)$$

where m is the modulation index of the inverter; θ is the vector angle of the output voltage; d, d_s, d_0 are the duty cycles of the output voltage active state, shoot-through state and zero voltage state, respectively.

III. MODELING AND ANALYSIS OF THE PROPOSE CONVERTER
The proposed converter can provide bi-directional power flow among SC, Li-battery and grid, as shown in Figure 2. And the converter can work in boost mode and buck mode.

A. BOOST MODE
During boost mode, the proposed converter boosts the low Li-battery voltage to high dc-link voltage. There are three work states: zero state, active state and shoot-through state.
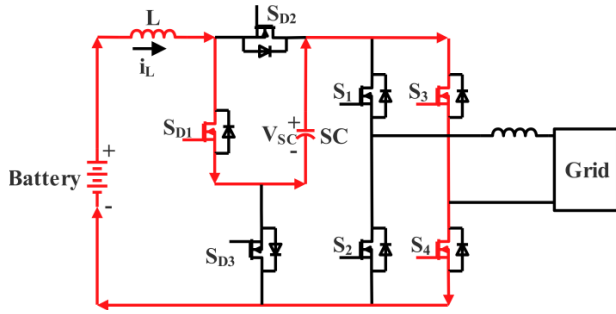
FIGURE 3. Flow path in shoot-through state of boost mode.

1) SHOOT-THROUGH STATE

In shoot-through state, the switches S_{D1} and S_3 & S_4 (S_1 & S_2) are turned ON while switches S_{D2} and S_{D3} are simultaneously turned OFF, as shown in Figure 3. In this state, the power is transferred from the Li-battery and SC to the inductor L. The state equation is given by:

$$\begin{cases} L\dfrac{di_L}{dt} = -(R_L + R_C)i_L + V_{SC} + V_B \\ C\dfrac{dV_{SC}}{dt} = -i_L \end{cases} \quad (2)$$

where V_B is the Li-battery voltage; V_{SC} is the SC voltage; I_L is the current through the inductor L; R_L and R_C are parasitic resistances of the inductor L and SC, respectively.

2) ACTIVE STATE

In active state, both switches S_{D2} and S_{D3} are turned ON while switches S_{D1} is simultaneously turned OFF, as shown in Figure 4. In this state, the Li-battery V_B and inductor L charge SC and power is transferred from the Li-battery V_B and inductor L to the grid. The state equation can be calculated as follows:

$$\begin{cases} L\dfrac{di_L}{dt} = -(R_L + R_C)i_L - V_{SC} + V_B + R_C i_O \\ C\dfrac{dV_{SC}}{dt} = i_L - i_O \end{cases} \quad (3)$$

where i_O is the output current.

3) ZERO STATE

In zero state, both switches S_{D2} and S_{D3} and S_1 & S_3 (S_2 & S_4) are turned ON while switches S_{D1} is simultaneously
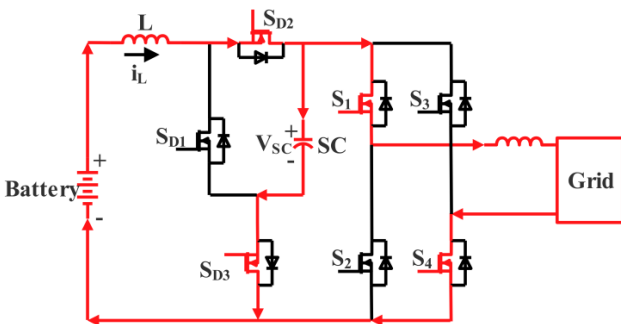

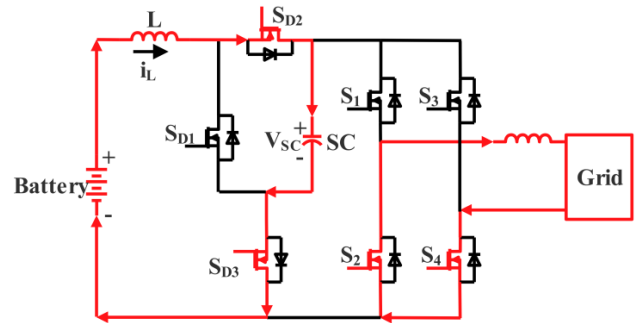**FIGURE 4.** Flow path in active state of boost mode.

FIGURE 5. Flow path in zero state of boost mode.

turned OFF, as shown in Figure 5. The state equation can be calculated as follows.

$$\begin{cases} L\dfrac{di_L}{dt} = -(R_L + R_C)i_L - V_{SC} + V_B \\ C\dfrac{dV_{SC}}{dt} = i_L \end{cases} \quad (4)$$

From equations (2) to (4), due to the average value of the inductor voltage and the capacitor current should be zero in one switching period of T_s, the voltage gain and current gain of the proposed converter in boost mode are as follows [26]:

$$\frac{V_{SC}}{V_B} = \frac{(1 - 2D_{boost})Z_H}{(1 - 2D_{boost})^2 Z_H + (2D_{boost}R_C + R_L)m} \quad (5)$$

$$i_L = \frac{m}{1 - 2D_{boost}} i_O \quad (6)$$

where, m is the modulation of the inverter; D_{boost} is the duty cycle in the shoot-through state; Z_H is high-voltage-side output impedance of the proposed converter:

$$Z_H = \frac{V_{SC}}{i_O} \quad (7)$$

From equation (2), the battery current ripple is as follows:

$$\Delta i_L = \frac{V_{SC} + V_B - (R_L + R_C)i_L}{L} D_{boost} T_S \quad (8)$$

According to the [27], the voltage gain of the conventional dc-dc half-bridge in boost mode is as follows:

$$\frac{V_{out}}{V_{in}} = \frac{(1 - D_t)Z_H}{(1 - D_t)^2 Z_H + R_L} \quad (9)$$

where, D_t is the duty cycle of the conventional dc-dc half-bridge.

Figure 6 shows the voltage gain in boost mode comparison between the conventional dc-dc half-bridge converter and the proposed converter. It can be seen that the voltage gain is greater than 1 when the duty cycle is changed from 0 to 0.5, and the voltage gain of the proposed converter is higher than that of the dc-dc half-bridge under the same R_L/Z_H ratio. Therefore, compared with the conventional dc-dc half-bridge converter, the topology proposed in this paper has a smaller duty cycle variation range and higher voltage gain.
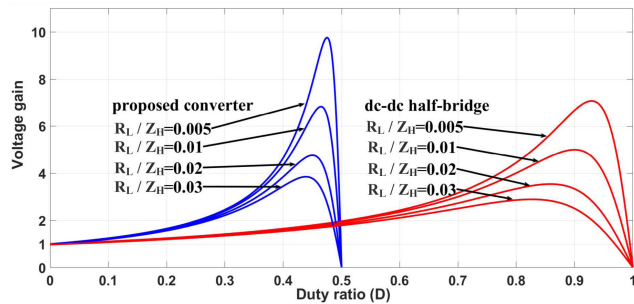
FIGURE 6. Voltage gain comparison between the conventional dc-dc half-bridge and the proposed converter in boost mode.

FIGURE 8. Flow path in shoot-through state of buck mode.

B. BUCK MODE

In buck mode, energy is transferred from the AC side to the DC side, and the single-phase full bridge converter operates in the rectification mode. Therefore, the dc link voltage is higher than the input AC voltage.

1) ACTIVE STATE AND ZERO STATE

In active state and zero state, the switches S_{D2} and S_{D3} are turned ON while switch S_{D1} is simultaneously turned OFF, as shown in Figure 7. In this state, the voltage of the DC bus is equal to the SC voltage, and power is transferred from the dc link to the Li-battery and inductor L. The state equation can be calculated as follows:

$$\begin{cases} L\dfrac{di_L}{dt} = -(R_L + R_{C1})i_L - V_{C1} + V_{SC} + R_{C1}i_O \\ C\dfrac{dV_{C1}}{dt} = i_L - i_O \end{cases} \tag{10}$$

$$V_{ocv} = R_{C1}i_L + V_{C1} - (R_{C1} + R_B)i_O \tag{11}$$

where, R_{C1} is the parasitic resistances of C_1; V_{ocv} is the open circuit voltage of the Li-battery; R_B is the internal resistance of the Li-battery [28]–[30].
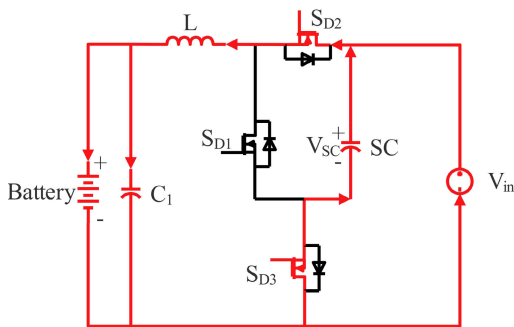

FIGURE 7. Flow path in active state and zero state of buck mode.

2) SHOOT-THROUGH STATE

In shoot-through state, the switches S_{D1} and S_3 & S_4 (S_1 & S_2) are turned ON while switches S_{D2} and S_{D3} are simultaneously turned OFF, as shown in Figure 8. In this state, the inductor L charges SC and Li-battery V_B. The power is transferred from inductor L to the Li-battery V_B and SC.
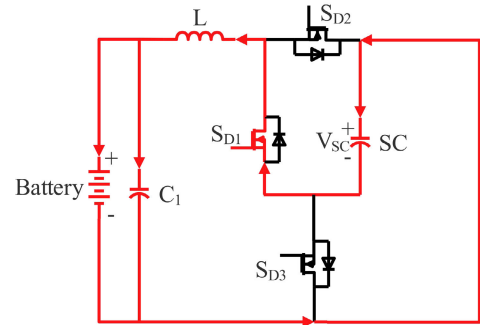
The state equation is given by:

$$\begin{cases} L\dfrac{di_L}{dt} = -(R_L + R_{C1})i_L - V_{C1} - V_{SC} + R_{C1}i_O \\ C\dfrac{dV_{C1}}{dt} = i_L - i_O \end{cases} \tag{12}$$

$$V_{ocv} = R_{C1}i_L + V_{C1} - (R_{C1} + R_B)i_O \tag{13}$$

From equations (10) to (13), the voltage gain of the proposed converter in buck mode is as follows:

$$\frac{V_{C1}}{V_{SC}} = \frac{(2D_{buck} - 1)Z_L}{Z_L + R_L} \tag{14}$$

$$i_o = i_L \tag{15}$$

where, D_{buck} is the duty cycle in the active state and zero state; Z_L is low-voltage-side output impedance of the proposed converter:

$$Z_L = \frac{V_{C1}}{i_O} \tag{16}$$

From equation (10), the battery current ripple is as follows:

$$\Delta i_L = \frac{V_{SC} - V_{C1} - (R_L + R_{C1})i_L + R_{C1}i_O}{L}D_{buck}T_S \tag{17}$$

Using the method mentioned in reference [27], the voltage gain of the conventional dc-dc half-bridge in the buck mode can be obtained:

$$\frac{V_{out}}{V_{in}} = \frac{D_t Z_L}{Z_L + R_L} \tag{18}$$

Figure 9 shows the voltage gain in buck mode comparison between the conventional dc-dc half-bridge and the proposed converter. As shown in Figure 9, the voltage gain is less than 1 when the duty cycle varies from 0.5 to 1. The proposed converter has stronger buck capability.

IV. SMALL SIGNAL MODELING ANALYSIS
A. BOOST MODE

The state-space average equation of the converter on one switching period can be obtained from (2) and (4). The equation are as follows:
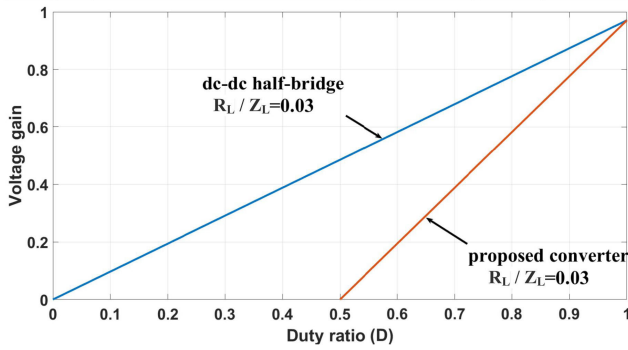
$$Kx' = A_1 x + B_1 u \tag{19}$$

FIGURE 9. Voltage gain comparison between the conventional dc-dc half-bridge and the proposed converter in buck mode.

where

$$A_1 = \begin{bmatrix} -(R_L + R_C) & 2D_{boost} - 1 \\ 1 - 2D_{boost} & 0 \end{bmatrix}, \quad u = \begin{bmatrix} V_B \\ i_O \end{bmatrix},$$

$$x = \begin{bmatrix} i_L \\ V_{SC} \end{bmatrix}, \quad K = \begin{bmatrix} L & 0 \\ 0 & C \end{bmatrix}, \quad B_1 = \begin{bmatrix} 1 & mR_C \\ 0 & -m \end{bmatrix}.$$

Using the perturbation method to establish a small signal model.

$$K\hat{x}' = A_1\hat{x} + B_1\hat{u} + C_1\hat{d} \qquad (20)$$

where $C_1 = \begin{bmatrix} 2V_{SC} - R_Ci_o \\ -2i_L + i_o \end{bmatrix}, \hat{u} = \begin{bmatrix} \hat{V}_B \\ \hat{i}_O \end{bmatrix}, \hat{x} = \begin{bmatrix} \hat{i}_L \\ \hat{V}_{SC} \end{bmatrix}.$

From the small signal model in (20), the duty cycle to SC voltage transfer function $G_{ud\_boost}(s)$ is shown in (21) at the bottom of the next page.

B. BUCK MODE

The state-space average equation of the converter on one switching period can be obtained from (10) to (13). The equations are shown as (22) and (23).

$$Kx' = A_1x + B_1u \qquad (22)$$
$$y' = Ex + Fu \qquad (23)$$

where

$$A_1 = \begin{bmatrix} -(R_L + R_{C1}) & -1 \\ 1 & 0 \end{bmatrix}, \quad u = \begin{bmatrix} i_O \\ V_{SC} \end{bmatrix},$$

$$x = \begin{bmatrix} i_L \\ V_{C1} \end{bmatrix}, \quad K = \begin{bmatrix} L & 0 \\ 0 & C \end{bmatrix}, \quad B_1 = \begin{bmatrix} R_{C1} & 2D_{buck} - 1 \\ -1 & 0 \end{bmatrix},$$

$$y = V_B, \quad E = \begin{bmatrix} R_{C1} & 1 \end{bmatrix}, F = \begin{bmatrix} -(R_{C1} + R_B) & 0 \end{bmatrix}.$$

Using the perturbation method to establish a small signal model.

$$K\hat{x}' = A_1\hat{x} + B_1\hat{u} + C_1\hat{d} \qquad (24)$$
$$\hat{y}' = E\hat{x} + F\hat{u} \qquad (25)$$

where $C_1 = \begin{bmatrix} V_{SC} \\ 0 \end{bmatrix}, \hat{u} = \begin{bmatrix} \hat{i}_O \\ \hat{V}_{SC} \end{bmatrix}, \hat{x} = \begin{bmatrix} \hat{i}_L \\ \hat{V}_{C1} \end{bmatrix}, \hat{y} = \hat{V}_B.$

The duty cycle to output voltage transfer function $G_{ud\_buck}(s)$ is shown in (26), at the bottom of the next page and the duty cycle to output current transfer function $G_{id\_buck}(s)$ is shown in (27), at the bottom of the next page.

C. DYNAMIC CHARACTERISTIC ANALYSIS

The pole-zero diagram of the duty cycle to SC voltage transfer function $G_{ud\_boost}(s)$ in boost mode is shown in Figure 10. Because all poles are placed in the left half plane, the system is open-loop stable. The zero point is in the right half plane, so the system is a non-minimum phase system [31]. As shown in Figure 10(a), one zero and two poles are close to the imaginary axis as the inductance increases. However, the effect of the zero point can be ignored because the distance from the zero point to the imaginary axis is much
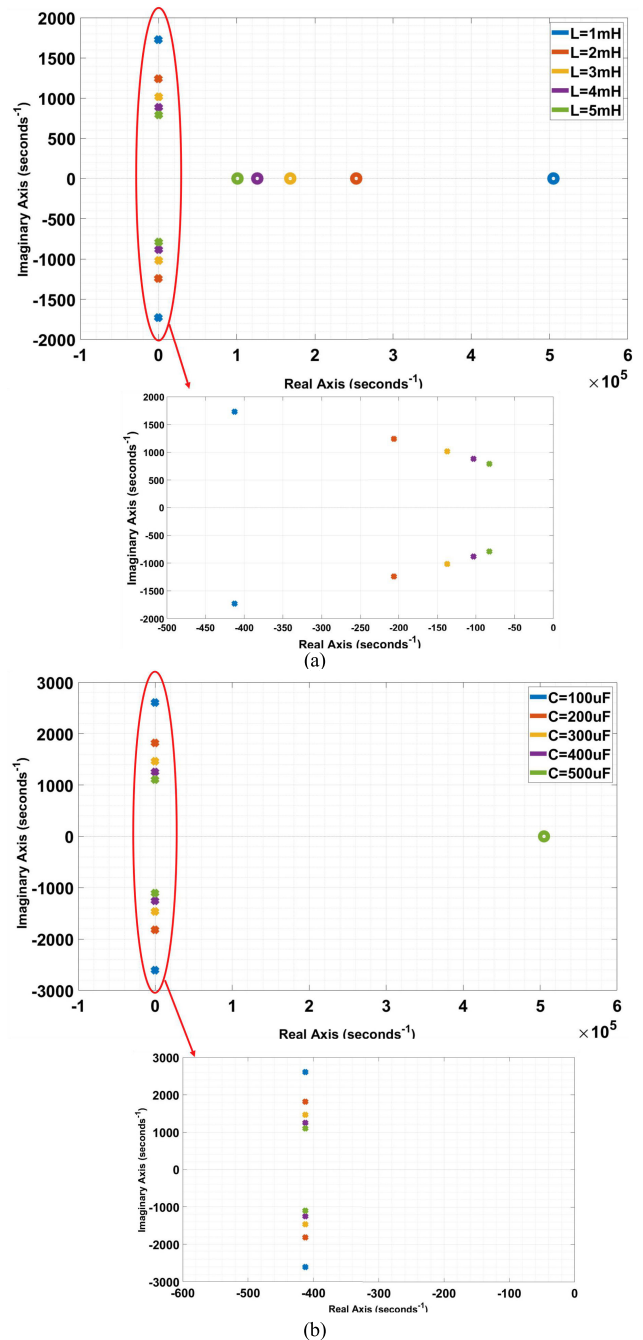

FIGURE 10. The pole-zero diagram of the duty cycle to SC voltage transfer function in boost mode. (a) Increased inductance. (b) Increased capacitance.

greater than the distance from the pole to the imaginary axis. Therefore, as the inductance increases, the non-minimum-phase overshoot increases and the adjustment time increases. As shown in Figure 10(b), when the capacitance is increased, the position of the zero point does not change while the pole is close to the real axis. The voltage overshoot decreases and the system settling time increases.

The pole-zero diagram of the duty cycle to output voltage transfer function $G_{ud\_buck}(s)$ in buck mode is shown in Figure 11. It can be seen that the system is open-loop stable. As shown in Figure 11(a), when the inductance is increased, the position of the zero point does not change while one pole is close to the imaginary axis and the other pole is far from the imaginary axis. When only the influence of the pole which is close to the imaginary axis is considered, the adjustment time of the system and the voltage overshoot increase as the inductance increases. As shown in Figure 11(b), as the capacitance increases, the zero and one pole are close to the imaginary axis and the other pole is far from the imaginary axis. The system rise-time decreases, and the voltage overshoot decreases.

V. CONTROL STRATEGY AND CONTROLLER DESIGN
A. CONTROL STRATEGY
The control strategy diagram of the proposed converter is shown in Figure 12. The control scheme includes four controllers. The SC voltage controller PI_1 outputs a duty cycle d_1 for controlling the SC voltage. The Li-battery current controller PI_2 and the Li-battery voltage controller PI_3 are two parallel controllers for controlling the charging current and voltage of the Li-battery. The controller PI_2 outputs a duty cycle d_2, and the controller PI_3 outputs a duty cycle d_3. The grid current controller PR outputs a duty cycle d_4. The PR controller can track the sinusoidal reference of the grid current [32]. The proposed controll strategy has two operation modes which are vehicles-to-grid (V2G) and grid-to-vehicles (G2V).

1) V2G MODE
In V2G mode, the flow chart of the control strategy is shown in Figure 13. The Li-battery and SC work together to supply the grid. When the required power of the grid P_G is equal to or less than the rated power of the Li-battery P_B. The energy required by the grid is mainly provided by the Li-battery. In this case, the d_1 obtains control of the shoot-through state

duty cycle d_s, and the d_4 obtains control of the active state duty cycle d.

In the stage of increased grid load, the power demand of the grid is higher than the Li-battery rated power. The SC meets the peak power demand of the grid in this condition. When the SC voltage is higher than $0.8V_{SC\_max}$, the voltage controller PI_1 works. When the SC voltage is lower than $0.8V_{SC\_max}$, the d_2 obtains control of the shoot-through state duty cycle d_s.

The energy stored in the capacitor depends on the voltage of the capacitor [3]:

$$E_c = \frac{1}{2}CV_c^2 \qquad (28)$$

From equation (28), when the capacitor voltage V_C is charged to 50% of the maximum voltage of the capacitor V_{C_max}, the capacitor stores only 25% of the energy. If the voltage closed loop stabilizes the capacitor voltage at 80% of the capacitor's maximum voltage, the capacitor store 64% of the energy. The reason for choosing the 80% voltage charging ratio is that the DC bus voltage will not drop greatly when the capacitor supplies power to the grid, and there is enough capacity to achieve voltage regulation of the DC bus.

2) G2V MODE
In G2V mode, energy flows from the grid to HESS. The flow chart of the control strategy is shown in Figure 14. The Li-battery is charged from constant current (CC) mode to constant voltage (CV) mode. The smaller one of the d_2 and the d_3 can obtain the control of the shoot-through-duty ratio d_s. When the d_2 obtain the control of the shoot-through-duty ratio d_s, the charger charges the Li-battery with a constant current I_{CC}. When the d_3 obtain the control of the shoot-through-duty ratio d_s, the charger charges the Li-battery with a constant voltage V_H.

The control block diagram of the Li-battery charger is shown in Figure 15. When the Li-battery voltage V_B is lower than the reference voltage V_H, d_3 is greater than d_2, so d_2 obtains control of the duty cycle d_s. The SBBBC is controlled by the current closed loop and I_o traces to its reference I_{CC}. At this time, the Li-battery voltage starts to rise. When the Li-battery voltage reaches the reference voltage V_H, the charging current is less than the I_{CC}. At this time d_2 is greater than d_3, so d_3 obtains control of the duty cycle d_s. The SBBBC is controlled by the voltage closed loop and V_B traces to its reference V_H.

$$G_{ud\_boost}(s) = \frac{\hat{V}_{SC}}{\hat{d}} = \frac{(1-2D_{boost})^2(2V_{SC}-R_Ci_o)-(sL+R_C+R_L)i_o}{(1-2D_{boost})[LCs^2+C(R_L+R_C)s+(1-2D_{boost})^2]} \qquad (21)$$

$$G_{ud\_buck}(s) = \frac{\hat{V}_{C1}}{\hat{d}} = \frac{2V_{SC}(R_{C1}R_BCS+R_B)}{LC_1(R_{C1}+R_B)s^2+[L+C(R_LR_{C1}+R_{C1}R_B+R_LR_B)]s+R_B+R_L} \qquad (26)$$

$$G_{id\_buck}(s) = \frac{\hat{i}_o}{\hat{d}} = \frac{2V_{SC}(R_{C1}CS+1)}{LC_1(R_{C1}+R_B)s^2+[L+C(R_LR_{C1}+R_{C1}R_B+R_LR_B)]s+R_B+R_L} \qquad (27)$$
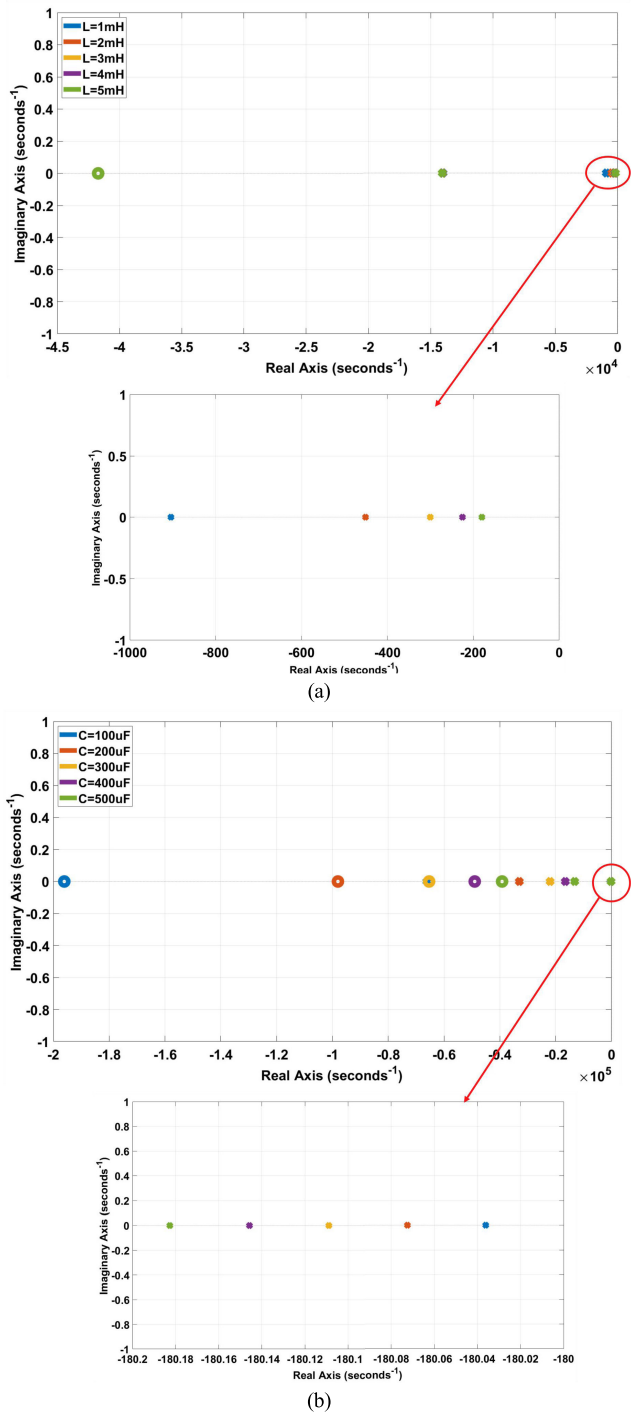
FIGURE 11. The pole-zero diagram of the duty cycle to output voltage transfer function in buck mode. (a) Increased inductance. (b) Increased capacitance.

When the charging current I_o is lower than $0.2I_{CC}$, the SC is charged. The control signals of switches S_{D1}, S_{D2} and S_{D3} are turned to zero to turn off these switches. The parallel diode of switch S_{D2} is reverse biased due to the increase in DC bus voltage. The Li-battery is removed from the circuit.
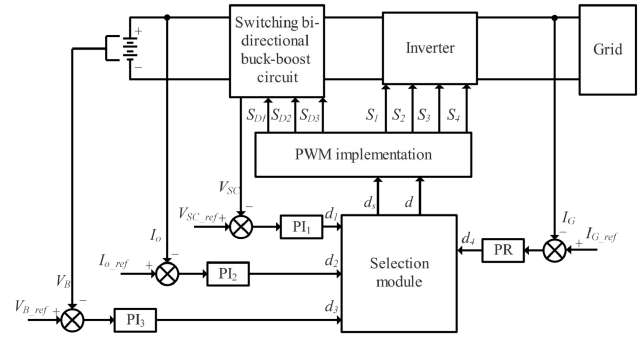

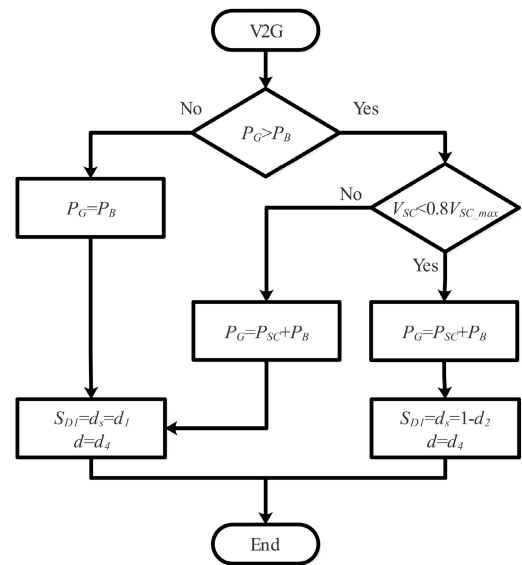**FIGURE 12.** The control strategy diagram.

FIGURE 13. The flow chart of the control strategy in V2G mode.

B. CONTROLLER DESIGN

According to the transfer functions given in Section IV, the bode diagram can be used to design the PI controller in the frequency domain.

The bode plot of the voltage loop in boost mode is shown in Figure 16. As shown in the open-loop bode plot, the amplitude margin is 17.1dB and the phase margin is 96.5°, which indicates that the closed-loop system is stable. The bode plot of the closed-loop transfer function shows that the output voltage can track the reference voltage with small error [33].

The bode plot of the current loop is shown in Figure 17 and the bode plot of the voltage loop in buck mode is shown in Figure 18. As shown in the open-loop bode plot of the voltage loop, the phase margin is 80.4°. The phase margin of the open-loop bode plot of the current loop is 70°. It can be seen that the system has a high stability margin. In order to obtain a good dynamic response, the appropriate cutoff frequency of the open-loop bode plot is 1kHz when the switching frequency of the converter is 10 kHz. As shown
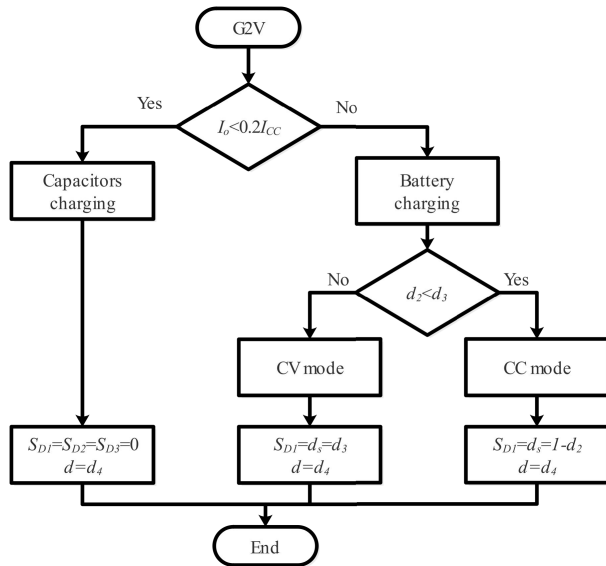
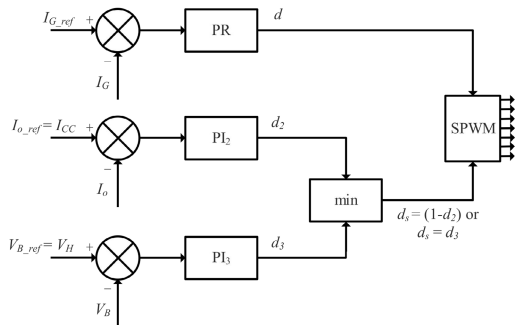**FIGURE 14.** The flow chart of the control strategy in G2V mode.

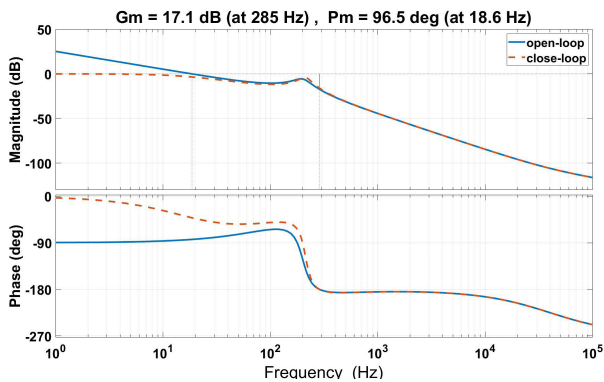**FIGURE 15.** Control block diagram of a Li-battery charger.

FIGURE 16. Bode plot of voltage loop in boost mode.

FIGURE 17. Bode plot of current loop in buck mode.
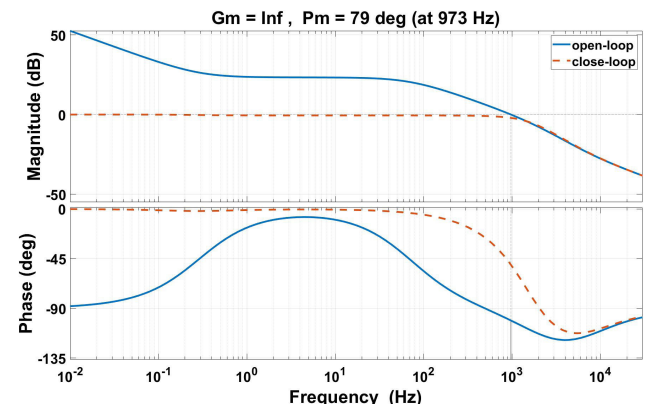
FIGURE 18. Bode plot of voltage loop in buck mode.

TABLE 2. Design papameters.

Parameter	Value	Unit
Li-battery voltage V_B	100	V
SC voltage V_{SC}	200	V
grid voltage V_G	100	V
grid voltage frequency	50	Hz
inductor L	2	mH
filter inductor L_f	2	mH
supercapacitor SC	2	F
parallel capacitance of the Li-battery C_1	470	μF
parasitic resistors R_L	800	mΩ
parasitic resistors R_C	25	mΩ
parasitic resistors R_{C1}	51	mΩ
internal resistance of the Li-battery R_B	100	mΩ
switching frequency f_s	5	kHz

in the bode plot of the closed-loop transfer function, the low-frequency closed-loop gain is low, so the tracking error is small.

VI. SIMULATION AND EXPERIMENTAL VERIFICATION
A. SIMULATION RESULTS
The SBBBC was simulated to verify the feasibility and dynamic performance. The simulation parameters are shown in Table 2.
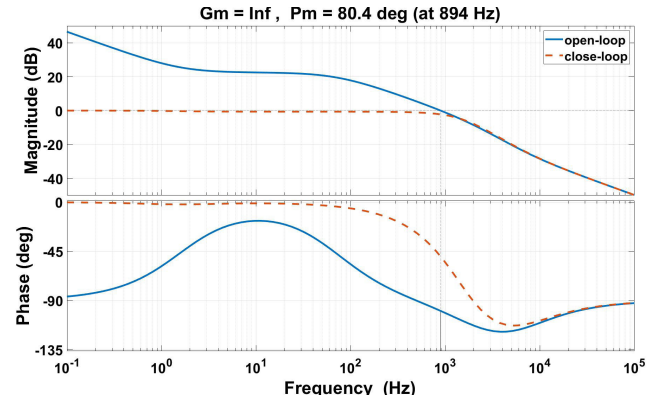
Figure 19 shows the simulation waveforms when the SBBBC is operating in boost mode. To make the grid current clear, the amplitude of the grid current is amplified 10 times. The current injected into the grid is in phase with the grid voltage to achieve a unit power factor. As shown in Figure 19(b), when the shoot-through duty cycle d_s is 0.25, the proposed converter boosts the 100V Li-battery voltage to 200V SC voltage, which meets the voltage gain given by equation (5). At $t = 0.5$, the reference current I_{G_ref} of
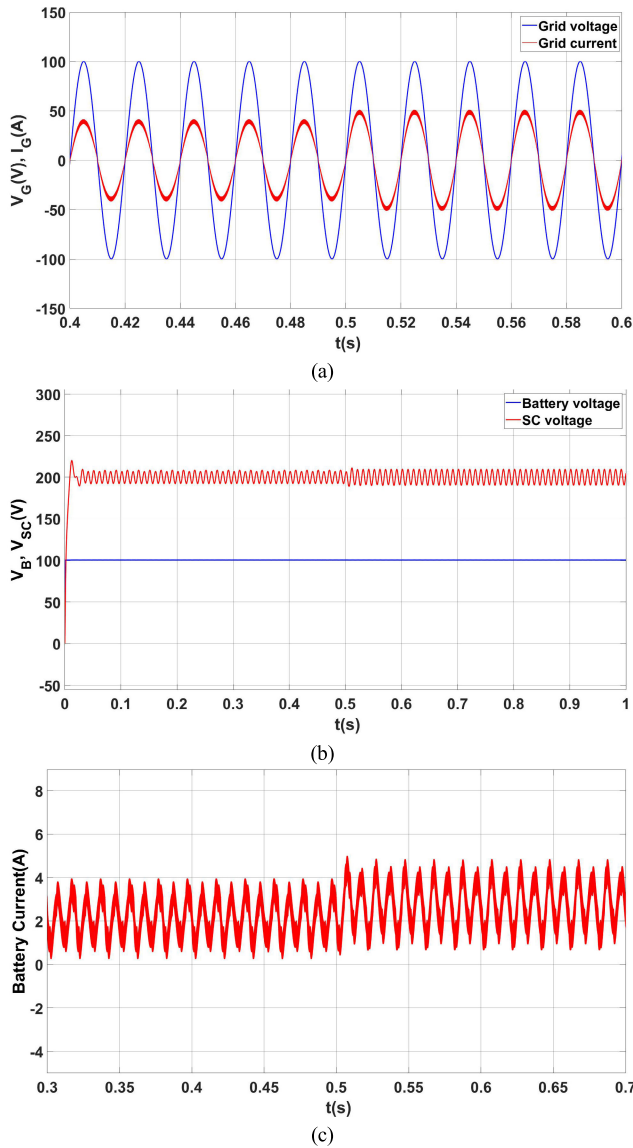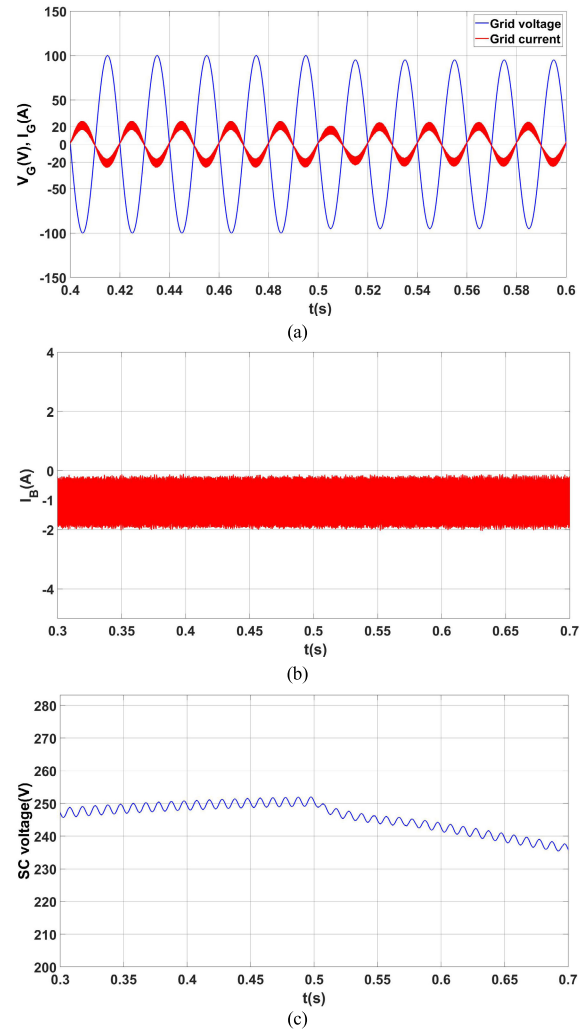
FIGURE 19. Simulation results of the proposed system. (a) Grid voltage and grid current. (b) Battery discharge voltage and SC voltage. (c) Battery discharge current.

the grid current controller changes from 4A to 5A. At this time, the Li-battery current increases and the output power of the Li-battery increases, which can achieve a fast response of the grid current. The capacitor voltage remains constant and the energy required by the grid is provided by the Li-battery.

Figure 20 shows the main waveforms when the SBBBC is operating in buck mode. To make the grid current clear, the amplitude of the grid current is amplified by 10 times. The grid current is in reverse phase with the grid voltage, so the energy flows from the grid to the HESS. At this time, the grid charges the energy storage system. At $t = 0.5$, the amplitude of grid voltage drops from 100V to 95V. As shown in Figure 20(a), when the grid voltage decreases, the grid current can quickly reach a stable state under the action of

FIGURE 20. Simulation results of the proposed system. (a) Grid voltage and grid current. (b) Battery charging current. (c) SC voltage.
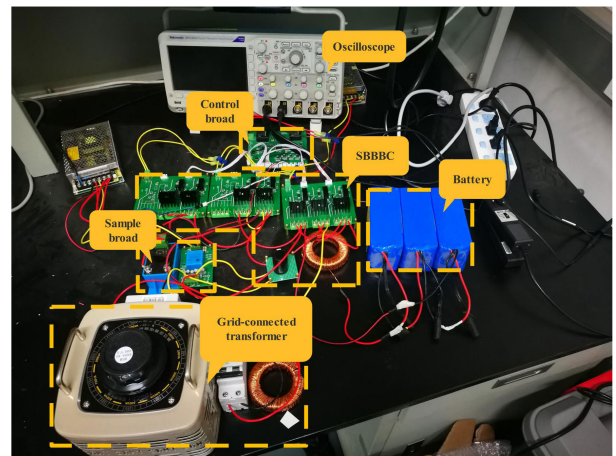
FIGURE 21. The experimental platform.

the grid-connected controller. The Li-battery charging current waveform is shown in Figure 20(b). It can be seen that the charging current of the Li-battery remains constant. As shown in Figure 20(c), the SC outputs energy to the Li-battery.
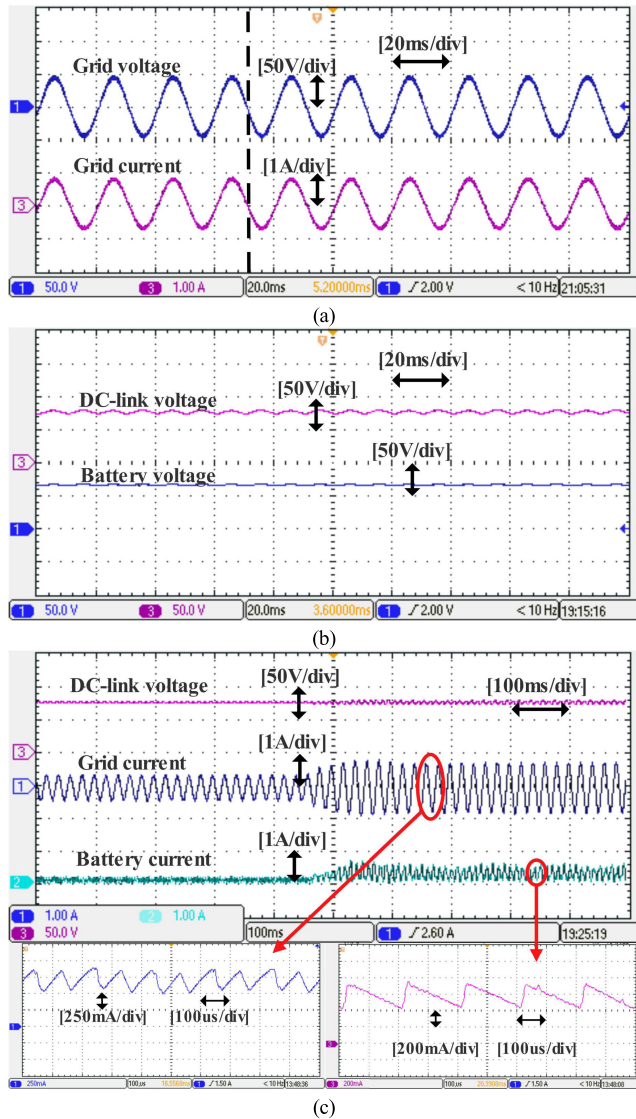
FIGURE 22. The experimental results of the boost mode. (a) Grid voltage and grid current. (b) Battery voltage and DC-link voltage. (c) Transient response waveform and current ripple waveform.

TABLE 3. Experimental parameters.

Parameter	Value	Unit
battery voltage	70	V
DC-link voltage	80	V
grid voltage	50	V
grid voltage frequency	50	Hz
filter inductor L_f	2	mH
switching frequency	5	kHz

B. EXPERIMENTAL RESULTS

A prototype of the proposed converter has been built to validate the electrical feasibility of the topology and the suitability of the designed controller, as shown in Figure 21. The parameters of the experimental device are given in Table 3.

The experimental results of the boost mode are shown in Figure 22. In Figure 22(a), it can be seen that the current
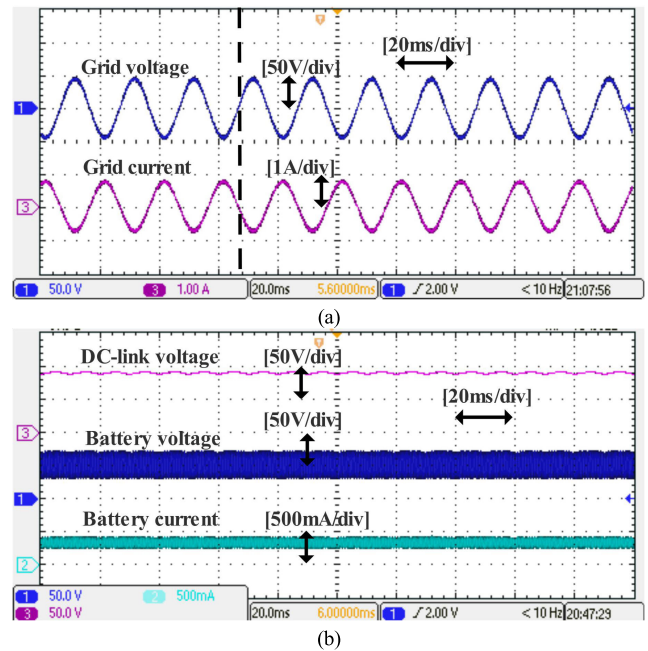

FIGURE 23. The experimental results of the buck mode. (a) Grid voltage and grid current. (b) Battery voltage, battery current and DC-link voltage.
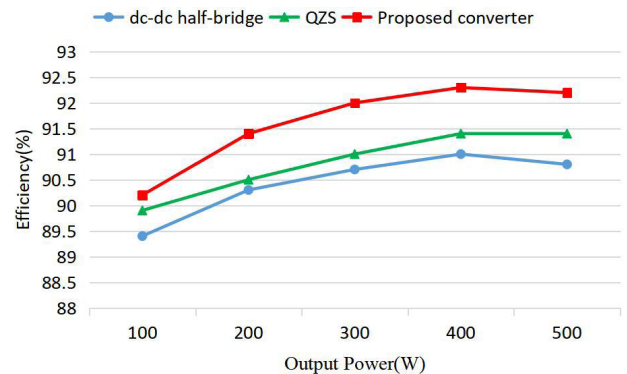

FIGURE 24. Efficiency comparison of three converters at load change.

and voltage of the grid are in phase, resulting in a unit power factor. At this time, the HESS provides energy to the grid. In Figure 22(b), when the shoot-through duty cycle d_s is 0.0625, the proposed converter boosts the 70V Li-battery voltage to 80V DC-link voltage, which meets the voltage gain given by equation (5). Figure 22(c) shows the transient response of the proposed topology when the grid current rises from 0.4A to 0.8A. It can be seen that the system can reaches steady state again in 20ms. The experimental results show that the designed controller has good dynamic performance. In Figure 22(c), the battery current ripple and grid current ripple of SBBBC are 25% and 30%, respectively.

The experimental results of the buck mode are shown in Figure 23. The voltage and current of the grid are in reverse phase, so the energy flows from the grid to the HESS. In Fig. 23(b), when the shoot-through duty cycle d_s is 0.11, the proposed converter steps down the 90V DC-link voltage to 70V Li-battery voltage, which meets the

TABLE 4. Comparison of three topologies.

Topology Features	dc-dc half-bridge	QZS	Proposed converter
Switchs	2	1	3
Requirement of dead time	Yes	No	No
EMI noise immunity	No	Yes	Yes
Voltage gain	1/(1-D)	1/(1-2D)	1/(1-2D)
Number of passive devices	2	4	2
Duty cycle variation range	0-1	0-0.5	0-0.5

voltage gain given by equation (14). The charging current of the battery remains constant.

C. COMPARISON WITH OTHER CONVERTERS

In Figure 24 and Table 4, the performance of SBBBC is compared with traditional dc-dc half bridges and qZSI. It can be seen that the efficiency of the proposed converter can reach 92.3%. Compared with the traditional dc-dc half bridge, SBBBC can significantly increase the voltage gain under the same duty-cycle. Similar to qZSI, SBBBC uses shoot-through as an operating state. Therefore, it does not require any dead time and is resistant to electromagnetic interference. Compared with qZSI, SBBBC has only two passive components, which can reduce the size of the device.

VII. CONCLUSION

This paper presents a SBBBC for V2G system. The proposed converter not only has high voltage gain and immunity to electromagnetic interference, but also provides a bidirectional energy flow path. In this paper, different working modes of the SBBBC are discussed in detail and the small signal model of the converter is established. The zero-pole diagram of the system was drawn, the dynamic characteristics of the system were analyzed and its stability was proved. This paper proposes control strategies for V2G and G2V modes, which implement energy management of the HESS. The controller is designed in the frequency domain, so that the controller has good dynamic performance. Finally, the correctness of the theory and the feasibility of the control strategy have been verified through simulations and experiments on laboratory prototypes.

REFERENCES

[1] F. Naseri, E. Farjah, and T. Ghanbari, "An efficient regenerative braking system based on battery/supercapacitor for electric, hybrid and plug-in hybrid electric vehicles with BLDC motor," *IEEE Trans. Veh. Technol.*, vol. 66, no. 5, pp. 3724–3738, May 2017.

[2] S. G. Wirasingha and A. Emadi, "Classification and review of control strategies for plug-in hybrid electric vehicles," *IEEE Trans. Veh. Technol.*, vol. 60, no. 1, pp. 111–122, Jan. 2011.

[3] J. Cao and A. Emadi, "A new battery/ultraCapacitor hybrid energy storage system for electric, hybrid, and plug-in hybrid electric vehicles," *IEEE Trans. Power Electron.*, vol. 27, no. 1, pp. 122–132, Jan. 2012.

[4] O. Hegazy, J. V. Mierlo, and P. Lataire, "Analysis, modeling, and implementation of a multidevice interleaved DC/DC converter for fuel cell hybrid electric vehicles," *IEEE Trans. Power Electron.*, vol. 27, no. 11, pp. 4445–4458, Nov. 2012.

[5] A. Khaligh and Z. Li, "Battery, ultracapacitor, fuel cell, and hybrid energy storage systems for electric, hybrid electric, fuel cell, and plug-in hybrid electric vehicles: State of the art," *IEEE Trans. Veh. Technol.*, vol. 59, no. 6, pp. 2806–2814, Jul. 2010.

[6] M. Ortuzar, J. Moreno, and J. Dixon, "Ultracapacitor-based auxiliary energy system for an electric vehicle: Implementation and evaluation," *IEEE Trans. Ind. Electron.*, vol. 54, no. 4, pp. 2147–2156, Aug. 2007.

[7] L. Gao, R. A. Dougal, and S. Liu, "Power enhancement of an actively controlled battery/ultracapacitor hybrid," *IEEE Trans. Power Electron.*, vol. 20, no. 1, pp. 236–243, Jan. 2005.

[8] L. Solero, A. Lidozzi, and J. A. Pomilio, "Design of multiple-input power converter for hybrid vehicles," *IEEE Trans. Power Electron.*, vol. 20, no. 5, pp. 1007–1016, Sep. 2005.

[9] M.-E. Choi, S.-W. Kim, and S.-W. Seo, "Energy management optimization in a battery/supercapacitor hybrid energy storage system," *IEEE Trans. Smart Grid*, vol. 3, no. 1, pp. 463–472, Mar. 2012.

[10] J. Shen and A. Khaligh, "Design and real-time controller implementation for a battery-ultracapacitor hybrid energy storage system," *IEEE Trans. Ind. Informat.*, vol. 12, no. 5, pp. 1910–1918, Oct. 2016.

[11] Y. Ghiassi-Farrokhfal, C. Rosenberg, S. Keshav, and M.-B. Adjaho, "Joint optimal design and operation of hybrid energy storage systems," *IEEE J. Sel. Areas Commun.*, vol. 34, no. 3, pp. 639–650, Mar. 2016.

[12] Z. Song, H. Hofmann, J. Li, X. Han, and M. Ouyang, "Optimization for a hybrid energy storage system in electric vehicles using dynamic programing approach," *Appl. Energy*, vol. 139, pp. 151–162, Feb. 2015.

[13] S. Hu, Z. Liang, and X. He, "Ultracapacitor-battery hybrid energy storage system based on the asymmetric bidirectional Z-source topology for EV," *IEEE Trans. Power Electron.*, vol. 31, no. 11, pp. 7489–7498, Nov. 2016.

[14] N. Qi, K. Dai, F. Yi, X. Wang, Z. You, and J. Zhao, "An adaptive energy management strategy to extend battery lifetime of solar powered wireless sensor nodes," *IEEE Access*, vol. 7, pp. 88289–88300, 2019.

[15] Z. Amjadi and S. S. Williamson, "Power-electronics-based solutions for plug-in hybrid electric vehicle energy storage and management systems," *IEEE Trans. Ind. Electron.*, vol. 57, no. 2, pp. 608–616, Feb. 2010.

[16] C. Zheng, W. Li, and Q. Liang, "An energy management strategy of hybrid energy storage systems for electric vehicle applications," *IEEE Trans. Sustain. Energy*, vol. 9, no. 4, pp. 1880–1888, Oct. 2018.

[17] H. H. Eldeeb, A. T. Elsayed, C. R. Lashway, and O. Mohammed, "Hybrid energy storage sizing and power splitting optimization for plug-in electric vehicles," *IEEE Trans. Ind. Appl.*, vol. 55, no. 3, pp. 2252–2262, May 2019.

[18] J. Fang, Y. Tang, H. Li, and X. Li, "A battery/ultracapacitor hybrid energy storage system for implementing the power management of virtual synchronous generators," *IEEE Trans. Power Electron.*, vol. 33, no. 4, pp. 2820–2824, Apr. 2018.

[19] C. Zhao, H. Yin, Z. Yang, and C. Ma, "Equivalent series resistance-based energy loss analysis of a battery semiactive hybrid energy storage system," *IEEE Trans. Energy Convers.*, vol. 30, no. 3, pp. 1081–1091, Sep. 2015.

[20] M. A. Khan, A. Ahmed, I. Husain, Y. Sozer, and M. Badawy, "Performance analysis of bidirectional DC–DC converters for electric vehicles," *IEEE Trans. Ind. Appl.*, vol. 51, no. 4, pp. 3442–3452, Jul./Aug. 2015.

[21] Y.-J. Lee, A. Khaligh, and A. Emadi, "Advanced integrated bidirectional AC/DC and DC/DC converter for plug-in hybrid electric vehicles," *IEEE Trans. Veh. Technol.*, vol. 58, no. 8, pp. 3970–3980, Oct. 2009.

[22] O. C. Onar, J. Kobayashi, D. C. Erb, and A. Khaligh, "A bidirectional high-power-quality grid interface with a novel bidirectional noninverted Buck–Boost converter for PHEVs," *IEEE Trans. Veh. Technol.*, vol. 61, no. 5, pp. 2018–2032, Jun. 2012.

[23] M. Aamir, S. Mekhilef, and H.-J. Kim, "High-gain zero-voltage switching bidirectional converter with a reduced number of switches," *IEEE Trans. Circuits Syst. II, Exp. Briefs*, vol. 62, no. 8, pp. 816–820, Aug. 2015.

[24] S. Hu, Z. Liang, D. Fan, and X. He, "Hybrid ultracapacitor–battery energy storage system based on Quasi-Z-source topology and enhanced frequency dividing coordinated control for EV," *IEEE Trans. Power Electron.*, vol. 31, no. 11, pp. 7598–7610, Nov. 2016.

[25] W. Liang, Y. Liu, B. Ge, H. Abu-Rub, R. S. Balog, and Y. Xue, "Double-line-frequency ripple model, analysis, and impedance design for energy-stored single-phase quasi-Z-source photovoltaic system," *IEEE Trans. Ind. Electron.*, vol. 65, no. 4, pp. 3198–3209, Apr. 2018.

[26] M. Nguyen, Y. Lim, and S. Park, "A comparison between single-phase quasi-Z-source and quasi-switched boost inverters," *IEEE Trans. Ind. Electron.*, vol. 62, no. 10, pp. 6336–6344, Oct. 2015.

[27] J. C. Rosas-Caro, F. Z. Peng, H. Cha, and C. Rogers, "Z-source converter based zero voltage electronic load," in *Proc. IEEE Power Electron. Spec. Conf.*, Jun. 2008, pp. 2764–2770.

[28] M. Einhorn, F. V. Conte, C. Kral, and J. Fleig, "Comparison, selection, and parameterization of electrical battery models for automotive applications," *IEEE Trans. Power Electron.*, vol. 28, no. 3, pp. 1429–1437, Mar. 2013.

[29] P.-J. Liu and C.-H. Yen, "A fast-charging switching-based charger with adaptive hybrid duty cycle control for multiple batteries," *IEEE Trans. Power Electron.*, vol. 32, no. 3, pp. 1975–1983, Mar. 2017.

[30] V. M. Iyer, S. Gulur, and S. Bhattacharya, "Small-signal stability assessment and active stabilization of a bidirectional battery charger," *IEEE Trans. Ind. Appl.*, vol. 55, no. 1, pp. 563–574, Jan. 2019.

[31] S. Liu, B. Ge, X. Jiang, H. Abu-Rub, and F. Peng, "Modeling, analysis, and motor drive application of quasi-Z-source indirect matrix converter," *COMPEL-Int. J. Comput. Math. Electr. Electron. Eng.*, vol. 33, nos. 1–2, pp. 298–319, Dec. 2013.

[32] D. Sun, B. Ge, W. Liang, H. Abu-Rub, and F. Z. Peng, "An energy stored quasi-Z-source cascade multilevel inverter-based photovoltaic power generation system," *IEEE Trans. Ind. Electron.*, vol. 62, no. 9, pp. 5458–5467, Sep. 2015.

[33] Y. Chen, S. Zhao, Z. Li, X. Wei, and Y. Kang, "Modeling and control of the isolated DC–DC modular multilevel converter for electric ship medium voltage direct current power system," *IEEE J. Emerg. Sel. Topics Power Electron.*, vol. 5, no. 1, pp. 124–139, Mar. 2017.
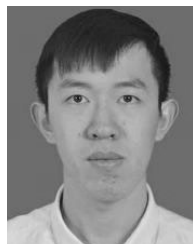
XU XIE is currently pursuing the M.S. degree in electrical engineering, with the Electrical and Control Engineering College, North China University of Technology, Beijing. His main areas of interest are switching converters and hybrid energy storage.

SHUO LIU received the Ph.D. degree in electrical engineering from Beijing Jiaotong University, Beijing, China, in 2015. He is currently an Associate Professor with the Electrical and Control Engineering College, North China University of Technology, Beijing. His research interests include Z-source converter, matrix converter, and motor drives.

LIYONG YANG is currently an Associate Professor with the Electrical and Control Engineering College, North China University of Technology, Beijing. His main research interests are the electrical machine drives and power electronics.

• • •